Heart Failure Reviews (2022) 27:1531–1541
https://doi.org/10.1007/s10741-021-10183-w

The utility of positron emission tomography in cardiac amyloidosis

Subha Saeed[1] · Jean Michel Saad[2] · Ahmed Ibrahim Ahmed[2] · Yushui Han[2] · Mouaz H. Al-Mallah[2,3]

Accepted: 14 October 2021 / Published online: 7 November 2021

Abstract

Cardiac amyloidosis, characterized by progressive restrictive cardiomyopathy, presents unusual diagnostic challenges. Conventional cardiac scintigraphy has shown limited utility in the quantification of disease burden and serial follow-up of cardiac amyloidosis. The advent of specialized positron emission tomography with specific amyloid-binding radiotracers has the potential to change currently employed diagnostic algorithms for the imaging of cardiac amyloidosis. This review aims to discuss the diagnostic utility of amyloid-binding radiotracers, including Pittsburg compound B, florbetapir, florbetapan, and sodium fluoride. These tracers have promising potential for the early detection of the particular type of cardiac amyloidosis, pursuing relevant medical intervention, assessing amyloid burden, monitoring treatment response, and overall prognostication.

Keywords Cardiac amyloidosis · Positron emission tomography · Cardiac scintigraphy · Pittsburg compound B · Florbetapir · Florbetapan · Sodium fluoride

Cardiac amyloidosis (CA) is characterized by extracellular deposition of misfolded filamentous proteins, derived primarily from circulating immunoglobulin light chains (AL) or transthyretin protein (ATTR) which clinically manifests as restrictive cardiomyopathy [1].

Imaging modalities like echocardiography and cardiac magnetic resonance (CMR) provide objective evidence of cardiac amyloidosis, which include the characteristic findings of increased ventricular wall thickness, diastolic dysfunction, delayed left ventricular gadolinium enhancement, and T-1 weighted images. These myocardial parameters help estimate the location and extent of amyloid deposition, but lack specificity for amyloidosis [2, 3]. Endo-myocardial biopsy (EMB) should have presumably filled this void in specificity, but along with its invasive nature, inability to predict disease burden and the uneven pattern of the amyloid deposition itself implies the limited utility of this modality [4]. Amyloid-binding radiopharmaceuticals in positron emission tomography may answer the diagnostic challenges presented by the progressive nature of heart failure associated with cardiac amyloidosis [5]. Because of their high sensitivity and specificity in early studies, these radiotracers have promising utility for early and accurate detection of CA, estimating disease burden, monitoring the treatment response, and prognostication [6].

The three main cardiac amyloidosis types include hereditary transthyretin amyloidosis (ATTRv-CA), wild-type ATTR amyloidosis (ATTRwt-CA), or immunoglobulin light chain amyloidosis (*AL-CA*)[7]. Nowadays, the management of CA has seen the development of targeted pharmaceutical therapy for ATTR-CA, including TTR stabilizers/silencers, and chemotherapy regimens for AL-CA, including anti-plasma cell therapies and anti-amyloid antibodies. These therapies are associated with slowing or halting cardiac amyloidosis progression, as such early recognition of cardiac amyloidosis remains of paramount priority so tailored therapy can be initiated accordingly [8]. In recent years, the giant leap forward was with non-invasive, nuclear scintigraphy imaging using bone-avid radiotracers, capable of binding micro-calcifications more commonly seen in ATTR-CA than AL amyloidosis [9]. This non-biopsy approach helped accurately diagnose ATTR-CA and differentiate the type of cardiac amyloidosis, with imaging modalities, discussed earlier and prompted a wide change in clinical approach and proposed diagnostic algorithm [10].

✉ Mouaz H. Al-Mallah
mal-mallah@houstonmethodist.org

[1] Crozer Keystone Health System, Upland, PA, USA

[2] Houston Methodist Debakey Heart & Vascular Center, Houston, TX, USA

[3] Weill Cornell Medical College, New York City, NY, USA

Limitations of cardiac scintigraphy

Currently, cardiac scintigraphy has left several clinical unmet needs in the management of cardiac amyloidosis. These include limitations in detecting the presence of early disease and the ability to monitor disease progression and/or response to therapy. These limitations have recently witnessed immense interest following the introduction of new disease-modifying therapies against cardiac amyloidosis [11].

High-grade tracer uptake in nuclear scintigraphy promised 100% specificity for ATTR-CA detection only in patients with established heart failure and in the presence of typical echocardiographic and CMR findings of advanced cardiac amyloidosis, implying limited sensitivity for the diagnosis of earlier stages of ATTR-CA [12]. Moreover, cardiac scintigraphy has primarily revolved around ATTR-CA diagnosis while neglecting other forms of CA such as AL amyloidosis [12, 13]. Using targeted amyloid-binding radiotracers, PET imaging provides the ability to detect all amyloid deposits regardless of original protein precursor. Early pilot studies using ^{11}C-PiB and ^{18}F-florbetapir have shown that PET may be able to detect AL-CA even before an increase in LV wall thickening or alterations in cardiac biomarkers [14, 15]. This would expand previously limited avenues in the diagnosis, monitoring, and management of AL cardiac amyloidosis.

Additionally, serial cardiac scintigraphy did not provide meaningful documentation of disease progression. Castano et al. thought to investigate the clinical feasibility of serial ^{99m}Tc-PYP cardiac scintigraphy in an attempt to quantify disease burden over time. This study included 20 ATTR-CA patients who underwent a second cardiac scintigraphy scan following an average of 1.5 years. The images were assessed and reported with both visual/semiquantitative and quantitative scores (H/CL). Albeit a clear disease progression based on clinical outcomes (progressive in NYHA class and/or death) and biomarkers (troponin and BNP), serial ^{99m}Tc-PYP cardiac scintigraphy failed to capture any differences over time [16].

This would suggest that cardiac scintigraphy would not mirror clinical course or increased disease burden and would be relegated for just the diagnosis of ATTR cardiac amyloidosis. As such, PET imaging using amyloid-binding radiotracer holds great potential in this field owing to the PET's ability to introduce improved quantification measures which might provide a clearer picture of disease burden and subsequently form the basis for monitoring of its progression or response to therapy (Fig. 1).

Amyloid-binding PET radiotracers

^{11}C-labeled Pittsburg compound-B (^{11}C-PiB)

^{11}C-PiB was one of the pioneering amyloid-fibril–binding radiotracers, initially developed to visualize and quantify β-amyloid plaques in Alzheimer's disease [17]. It was not long before ^{11}C-PiB found application for in vivo and in vitro visualization of cardiac amyloidosis were significantly increased. ^{11}C-PiB retention index (RI) was observed in both major types of CA, as compared to controls subjects [18, 19]. A subsequent study using measures of maximal and mean myocardium-to-blood cavity standard uptake value (SUV) ratios also found significant margins for differentiating between chemotherapy naïve AL-CA patients, compared to AL-CA patients with prior chemotherapy. This warranted recognition for ^{11}C-PiB as a surrogate indicator for detecting active ongoing light chain deposition in the myocardium. The study also served to propose possible prognostic utility of myocardial amyloid uptake [20].

Cardiac amyloid load is a prognostic marker in AL-CA, especially for chemotherapy-responsive patients with amyloid light chain (AL) load of less than 20% having better overall survival [21]. This non-invasive modality may help assess the dynamics of amyloid turnover in response to directed therapy. Furthermore, the degree of ^{11}C-PiB uptake may serve as an independent predictor and prognostic indicator for clinical events like all-cause mortality or acute decompensated heart failure on subsequent follow-up (Fig. 2) [6].

Of further interest was using ^{11}C-PiB among patients with genetically and histopathologically diagnosed neuropathic ATTRv-CA with ATTR V30M variant but without characteristic morphological features on ATTRv-CA on echocardiography [22]. The V30M variant of ATTRv-CA has two major phenotypes: early-onset disease (type B fibrils, with mainly have neuropathic manifestations) and late-onset disease (type A fibrils, with both cardiac and neurological manifestations) [23]. Although all patients with either fibrils type had significantly increased ^{11}C-PiB uptake compared to healthy controls, the measured ^{11}C-PiB RI was three times higher in type B fibrils than type A fibrils, implying that there is limited utility in measuring the magnitude of ^{11}C-PiB RI in ATTR patients. The increased ^{11}C-PiB RI in ATTR patients may be due to ^{11}C-PiB high binding affinity for type B fibril, rather than associated with true amyloid burden or predicting risk of cardiomyopathic development [22].

In contrast, cardiac scintigraphy showed increased DPD uptake in type A variant V30M ATTRv-CA and non-V30M ATTRv-CA, and absent uptake in type B

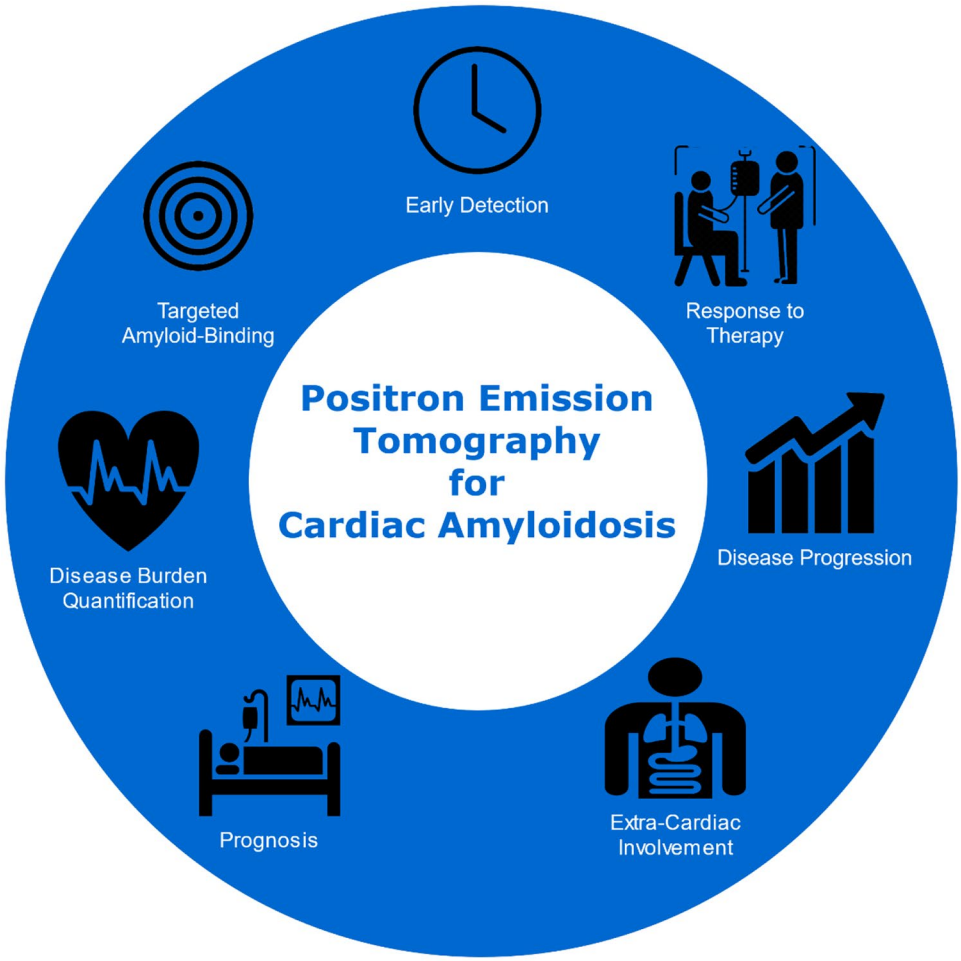

Fig. 1 Potential utility of positron emission tomography in the imaging of cardiac amyloidosis

variant V30M-ATTRv-CA further implying that positive DPD scintigraphy in ATTRv is associated with the future development of amyloid cardiomyopathy [22, 24]. If used together with TTR gene testing, the level and pattern of ^{11}C-PiB and DPD retention may help in the accurate subclassification of the ATTRv-CA fibril type and differentiate AL-CA from ATTRwt-CA, since ^{11}C-PIB showed uptake in all ATTR-CA and AL-CA cases while DPD is negative in certain ATTRv-CA [24].

A follow-up study found that ^{11}C-PiB uptake, analyzed by visual inspection and quantitative measures of SUV and RI, had significant diagnostic accuracy in discriminating main cardiac amyloidosis subtypes in biopsy-confirmed patients from healthy controls [25]. ^{11}C-PiB uptake was significantly higher in AL-CA than ATTR-CA, suggesting that the fibril type in ATTR-CA was affecting the ^{11}C-PiB binding to amyloid and subsequent visual and quantitative assessments [25]. Cardiac amyloidosis patients without cardiac wall hypertrophy had significantly increased ^{11}C-PIB uptake compared to controls, indicating that ^{11}C-PiB can detect early stages of cardiac amyloidosis before any overt morphological change, the basis of echocardiographic and CMR imaging [25].

However, ^{11}C-PiB binding to cardiac amyloids is variable with some degrees of reversibility in the retention index, thus requiring early imaging for accurate results [18]. In addition, the much shorter half-life of the ^{11}C-PIB radiotracer, compared to ^{18}F-labeled PET tracers, requires an on-site cyclotron for its continuous production and diagnostic utilization, which may be beyond the scope except in specialized centers [25].

^{18}F-Florbetapir

Preliminary studies established the promising potential for ^{18}F-florbetapir to serve as a molecular imaging biomarker for cardiac amyloidosis. ^{18}F-Florbetapir is hypothesized to directly bind to amyloid fibrils and thus causing longer tracer transit time—both features hinting at its diagnostic and quantitative abilities in assessing disease burden [26]. ^{18}F-Florbetapir belongs to the stilbene class of PET tracers. Earlier studies identified at least six surface- and

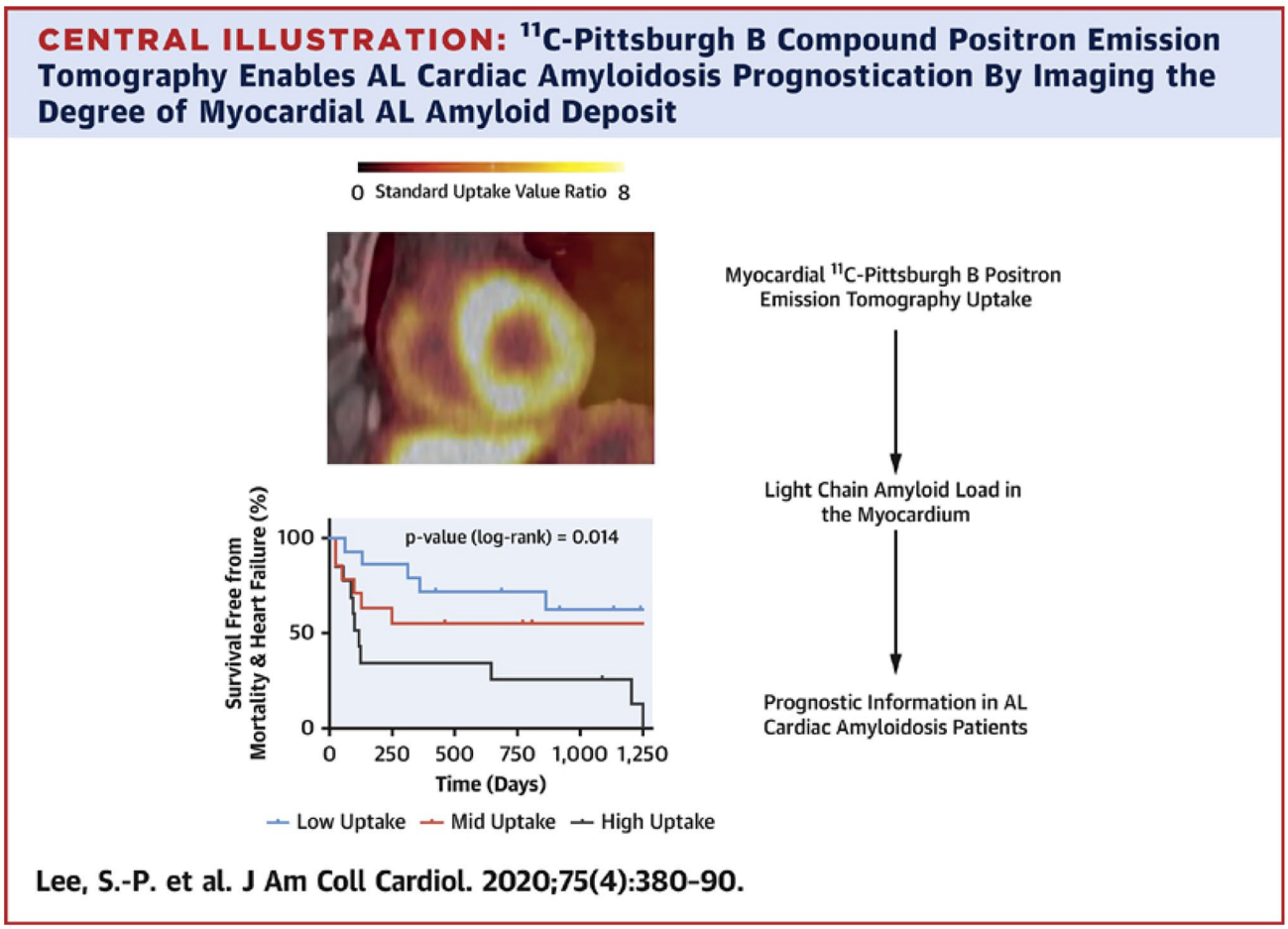

Fig. 2 The degree of myocardial ^{11}C-Pittsburgh B compound positron emission tomography uptake reflects the degree of myocardial amyloid deposit on invasive endomyocardial biopsy. Noninvasive evaluation of the degree of myocardial amyloid load can independently predict clinical outcome in AL cardiac amyloidosis patients. (Reuse permission obtained from [6])

core-binding sites in fibrils of neuritic amyloid-β plaques in autopsied Alzheimer's disease brain tissue, and a further three-binding-site model boasted a nanomolar affinity for a primary high-affinity site [27]. This characterization encouraged extrapolation of its application to cardiac amyloidosis as the beta-pleated motif of amyloid protein remains the same, irrespective of the precursor protein [28].

Earlier autoradiography studies on autopsy-confirmed AL-CA, ATTR-CA, and non-amyloid control samples demonstrated significantly increased ^{18}F-florbetapir–specific uptake in AL and ATTR samples as compared to controls [29]. Furthermore, significantly increased ^{18}F-florbetapir–specific uptake was seen in AL-CA samples compared to ATTR-CA (2.48 ± 0.40 versus 1.52 ± 0.22 DPM/mm^2; $p < 0.001$), despite overall significantly lower amyloid deposition burden in AL-CA samples as compared to ATTR-CA samples on histology [29]. Unlike the left ventricle myocardial standardized uptake values (SUV), target-to-blood pool ratio (TBR), and LV myocardium-to-liver SUV ratio, ^{18}F-florbetapir myocardial retention index (RI) and liver and cardiac time-activity curves (TACs) are kinetic parameters shown to effectively stratify AL-CA from ATTR-CA [30, 31]. Of significance is the semi-quantitative and incremental value of increased ^{18}F-florbetapir binding in samples with focal and limited amyloid deposits (in the absence of characteristic increased left ventricular wall thickness and increased left ventricular mass on echocardiogram) as compared to controls, signifying its utility in early diagnosis of cardiac amyloidosis [29]. Another study found a strong correlation between cardiac amyloidosis structural parameters (left ventricular wall thickness and left ventricular mass on echocardiography and extracellular volume on CMR), cardiac functional parameters (e.g., LVEF, global longitudinal strain, and relative apical sparing on echocardiogram), and myocardial ^{18}F-florbetapir retention index (RI) as a direct measure of cardiac amyloid burden in three groups of active AL-CA, remission AL-CA, and active systemic AL amyloidosis in the absence of CA (active-non-CA). The study also established ^{18}F-florbetapir RI's ability to discern the small

degree of myocardial amyloid burden in the active-non-CA group without established structural and functional markers of amyloidosis [15].

These studies potentiated the utility of ^{18}F-florbetapir as the litmus test to diagnose, differentiate, and assess the burden of cardiac amyloidosis. It may be worthwhile to consider dual-imaging with bone avid radiotracers and ^{18}F-florbetapir to diagnose cardiac amyloidosis and identify the type because the former modality has a higher affinity for ATTR-CA and the latter for AL-CA [29]. However, interval imaging with ^{18}F-florbetapir in AL-CA treatment-naïve patient before starting therapy and after chemotherapy completion with complete hematological response did not show a significant difference in RI or SUV_R, making it a less reliable marker to assess treatment response [32].

^{18}F-Florbetapan

Similar to ^{18}F-florbetapir, PET imaging with ^{18}F-florbetapan had demonstrated utility in accurate detection of b-amyloid neuritic plaques in Alzheimer's disease before feasibility studies were pursued to diagnose cardiac amyloidosis [33]. Qualitative and quantitative measures, including mean standardized uptake value (SUV) of LV myocardium, TBR-SUV ratio, and ^{18}F-florbetapan retention (percentage mean myocardial SUV change on scheduled time intervals) were significantly higher in CA patients as compared to control subjects. Initial studies identified the potential for ^{18}F-florbetapan to differentiate between non-CA, AL-CA, and ATTR-CA since AL-CA had a higher myocardial SUV variability spherical volume of interest (VOI) and higher myocardial tracer retention (MT–) cut-off [34–36]. Expectantly, ^{18}F-florbetapan retention in cardiac amyloidosis was an independent determinant of cardiac dysfunction on echocardiogram and cardiac magnetic resonance imaging (CMR), for functional and morphological parameters, like global LV longitudinal strain and ventricular wall thickness, respectively [34, 35]. Myocardial tracer retention (MTR) and changes in MTR over time (ΔMTR) were noted to correlate with disease progression and amyloid burden quantification, a promising potential for use in treatment response measurement [35].

A recent study investigated the utility of ^{18}F-florbetapan dynamic PET acquisition technique, whereby four 10-min static scans were obtained at pre-determined intervals after radiotracer injection [37]. A significant difference was found in the retention index among patients with AL-CA compared to ATTR-CA patients and non-CA individuals, with AL-CA patients having persistent, high cardiac uptake in all static scans, in contrast, while ATTR-CA patients and non-CA individuals showed a temporal decline in radiotracer uptake after early static scans (Fig. 3) [37].

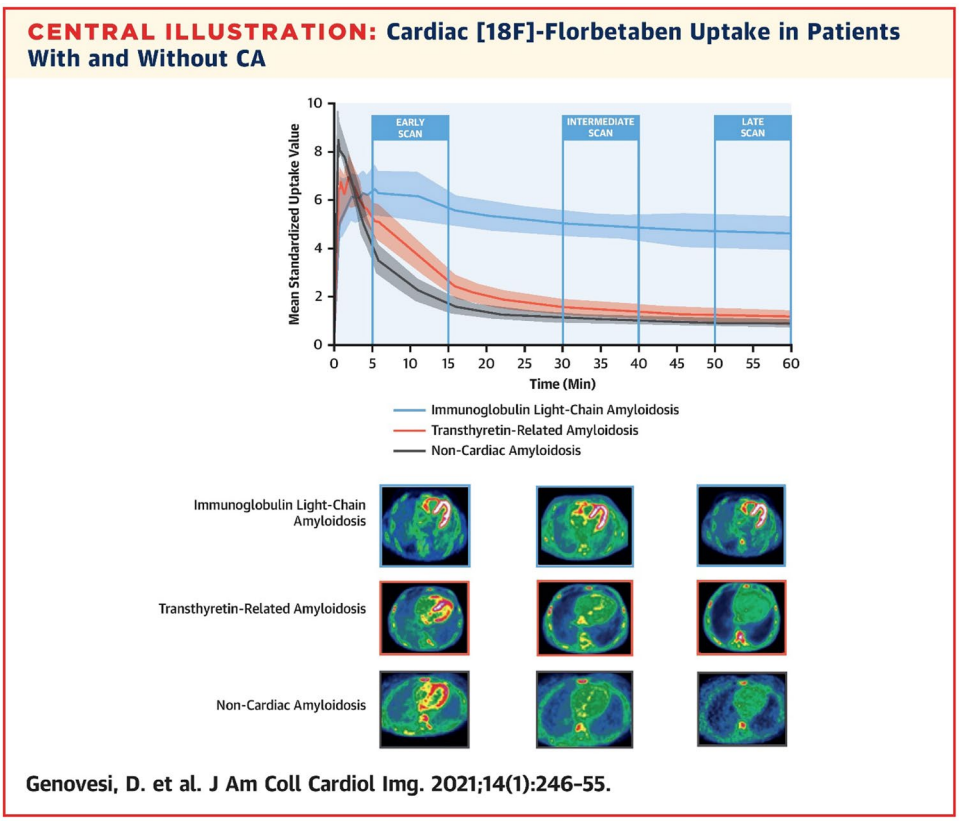

Fig. 3 (Upper panel) Fluorine 18 [18F]-florbetaben cardiac positron emission tomography myocardial time–activity curves in patients with immunoglobulin light-chain amyloidosis (AL) (blue), transthyretin-related amyloidosis (ATTR) (red), and non-cardiac amyloidosis (non-CA) (gray). The 95% confidence interval is represented as a shaded area for each curve. (Lower panel) Early (5 to 15 min), intermediate (30 to 40 min), and late (50 to 60 min) [18F]-florbetaben cardiac positron emission tomography scans in patients with AL and ATTR CA and those with non-CA. SUVmean ¼ mean standardized uptake value. (Reuse permission obtained from [37])

^{18}F-Sodium fluoride (^{18}F-NaF)

As outlined previously, positron emission tomography (PET) has amassed a wide array of novel radiotracers (^{18}Fluorine-labeled florbetapor/florbetapir and ^{11}Chlorine-labeled Pittsburg B) capable of imaging and quantifying cardiac amyloidosis (CA). However, currently, these radiotracers are yet to be approved for clinical use and are only available in limited specialized centers.

^{18}F-Sodium fluoride (^{18}F-NaF), on the other hand, is a readily available and FDA-approved tracer used primarily for the imaging of cancer metastasis especially prostate cancer. ^{18}F-NaF, a PET radiotracer, should in theory offer higher resolution imaging compared to Tc-labeled cardiac scintigraphy and more importantly the ability to obtain quantification of amyloid burden. Thus, similar to other quantitative measurements, this would allow for the earlier detection of cardiac amyloidosis, a more accurate assessment of amyloid disease burden, and response to therapies.

The use of ^{18}F-NaF PET for the imaging of cardiac amyloidosis was reported in the form of a case report by Van Der Gucht et al. which revealed this modality's potential to identify and differentiate ATTRv (Val122Ile) vs AL amyloidosis. More importantly, the authors highlighted that this technique was more efficient than comparable HMDP imaging citing faster kinetics and overall faster imaging protocols (20- and 60-min imaging acquisitions post-injections) [38]. However, another case report by Gagliardi et al. reported no ^{18}F-NaF uptake in 2 patients with ATTRwt and ATTRv (Ile68Leu). The authors hypothesized that ^{18}F-NaF uptake might not only be subject to differences in amyloid subtype (ATTR vs AL) but also specific TTR mutations [39]. It should be noted that the former case report was done prospectively compared to the latter which was done retrospectively in patients primarily evaluated for prostate cancer [38, 39].

A pilot study conducted by Morgenstern et al. confirmed the finding reported by Van Der Gucht et al. The study consisted of a small cohort of 5 ATTR (3 ATTRwt and 2 Val-122Ile), 2 AL, and 5 control patients (prostate cancer). PET along with CT-based attenuation images were acquired at 10- and 60-min (one study at 90 min) post-injection of 10 mCi of ^{18}F-NaF. Next, the scans were assessed both visually and quantitatively with standard uptake values in the entire myocardium (SUV_m). Specifically, SUVs were obtained for the entire myocardium and in the 17-segment cardiac model. ^{18}F-NaF uptake was absent in patients with AL and controls compared to ATTR-CA patients who showed a noticeable uptake, particularly in ATTRwt patients. Moreover, based on quantitative assessment of ATTR patients reported higher SUV_m vs AL and control patients. ^{18}F-NaF was noted to

Table 1 At a glance: summarizing the diagnostic utilities and applications of semiquantitative parameters in cardiac amyloidosis

Radiotracer	Semiquantitative parameter	Clinical utility
^{11}C-PiB	Retention index, visual uptake, SUV	Effectively differentiates cardiac amyloidosis, (ATTR and AL) from controls 100% accuracy in AL-CA Detects early stages of AL-CA in suspected cases [20]
	Maximal SUV	*Used together with ^{99m}Tc-PYP Scintigraphy*: *Complementary Relation*- Effective detection and differentiation of three major types of cardiac amyloidosis[57]
	Myocardial-to-blood SUV	*Assess dynamics of amyloid turnover*: differentiates between chemotherapy naïve AL-CA compared to prior chemotherapy, may serve as *predictor* of disease burden and *prognostic indicator*[18]
^{18}F-florbetapir	VU, RI, TBR, SUV, Cardiac TAC	Effectively differentiates cardiac amyloidosis, (ATTR and AL) from controls [30, 31]
	Maximum signal intensity in ROI (*autopsy subjects*)	Effectively differentiates cardiac amyloidosis, (ATTR and AL) from controls [29] Screen for early detection of AL-CA and ATTR-CA
	Cardiac TAC and RI	Discriminate AL-CA from ATTR-CA
	Cardiac RI	Assess amyloid burden in AL-CA [15], however, a less reliable marker for assessing treatment response [32]
^{18}F-florbetaben	SUV, retention index, Visual uptake	Effectively differentiates cardiac amyloidosis, (ATTR and AL) from controls [34] RI is an independent determinant of myocardial dysfunction
	MTR ΔMTR	Correlated with cardiac dysfunction on CMR and echocardiogram Discriminates AL-CA from ATTR-CA and control (MTR and SUV) *Treatment response measurement*: correlated with amyloid burden and disease progression [35]
	Cardiac RI	Discriminates AL-CA from ATTR-CA or other mimicking conditions [37]
^{18}F-NaF	*M/B or TBR*	Differentiates ATTR-CA from AL-CA *albeit with less sensitivity as cardiac scintigraphy* *Current clinical utility is still unclear and limited in the evaluation of cardiac amyloidosis*

be diffuse with varied uptake in different cardiac segments. SUV_m for ATTR patients was around 1.5*SUV_m of controls ($p=0.012$) and AL patients ($p=0.078$). Although the difference between ATTR and AL SUV_m approached but did not reach significance, this can be attributed to the small sample size used in the study [40].

These findings echoed a study by Trivieri et al. which used a hybrid PET/MR imaging approach. Diffuse ^{18}F-NaF uptake was observed in patients with ATTR (4) but not in AL (3) or control (7) patients. ^{18}F-NaF uptake colocalized with regions of LGE and correlated well with native T1 mapping [41]. A larger ^{18}F-NaF PET/MRI study (16 ATTR and 7 AL patients) showed that myocardial-to-blood pool (M/B) ratios were significantly higher in ATTR patients compared to AL patients ($p=0.001$) [42].

Although semiquantitative measures were able to distinguish ATTR from AL, the same was not true for visual qualitative assessments [40–43]. A study by Martineau et al. revealed that visual assessment of ^{18}F-NaF uptake in ATTR patients was limited due to its low sensitivity of 57% (specificity of 100%). ^{18}F-NaF uptake was significantly higher in ATTR compared to AL or controls; nevertheless, uptake was quite mild and inferior to that of blood pool in 57% of the studies which will undoubtedly complicate visual assessments [43].

Table 2 Summarizing key studies of the diagnostic value of ^{11}C-PiB PET imaging for cardiac amyloidosis

	Acquisition	Patient cohort	Parameters	Notes
Antoni et al. [18]	^{11}C-PiB PET/CT 15–25-min dynamic scan/ summed images at 10–15 s	3 ATTR 7 AL 5 Control	Visual assessment Cardiac RI	•Uptake was noted in all cardiac amyloidosis patients and none in the control •^{11}C-PiB RI didn't correlate with MBFs
Lee et al. [20]	^{11}C-PiB PET/CT 30-min post-injection + 3 min/bed	15 AL (5 underwent chemotherapy) 7 Control	Visual assessment Myocardium TBR	•Uptake was noted in 13/15 of cardiac amyloidosis patients and none in the control •M/B significantly different: CA > non-CA and chemotherapy naïve > chemotherapy
Pilebro et al. [22]	^{11}C-PiB PET/CT 25-min dynamic scan/ summed images at 15–25 min	10 ATTRv (V30M: 5 Type-A and 5 Type B fibrils) 5 Control	Visual assessment Cardiac RI	•Uptake was noted in all cardiac amyloidosis patients and none in the control •^{11}C-PiB significantly higher in type B vs type A fibrils
Ezawa et al. [19]	^{11}C-PiB PET/CT 30-min post-injection + 2 min/bed	7 ATTRv 1 Asymp. TTR carrier 7 AL 3 Control	Visual assessment	•^{11}C-PiB uptake is noted in several organ systems and can be used to work up systemic amyloidosis
Rosengren et al. [14]	^{11}C-PiB PET/CT 35-min dynamic scan/ summed images at 10–20 min	Retrospective Arm 21 ATTR (16 wt and 5v) 15 AL 15 Control	Visual assessment Cardiac RI SUV ration (SUV_R)	•Uptake was noted in all cardiac amyloidosis patients and none in the control •Sensitivity and specificity of SUV_R and RI for differentiation of CA vs control were 94%/93% and 94%/100% respectively
Takasone et al. [24]	^{11}C-PiB PET/CT 30-min post-injection + 2 min/bed	30 ATTR (8wt and 22v) 17 AL	Visual assessment Maximal SUV (SUV_{Max})	•(+) ^{99m}Tc-PYP and (−) ^{11}C-PiB PET seen in ATTRwt-CA •(−) ^{99m}Tc-PYP and (+) ^{11}C-PiB PET seen in AL-CA •PYP or CiB patterns were able to distinguish different ATTRv mutations
Lee et al. [6]	^{11}C-PiB PET/CT 30-min post-injection + 3 min/bed	41 AL 14 Control	SUV	•The degree of ^{11}C-PiB reflects cardiac amyloid burden •^{11}C-PiB uptake is an independent predictor of clinical outcomes in AL-CA

Table 3 Summarizing key studies of the diagnostic value of ^{18}F-florbetapir PET imaging for cardiac amyloidosis

	Acquisition	Patient cohort	Parameters	Notes
Park et al. [29]	Autoradiography study	Autopsy samples 10 ATTR 10 AL 10 Control	Total and nonspecific binding of ^{18}F-florbetapir	•Mean ^{18}F-florbetapir–specific uptake was significantly higher in CA > controls, AL > ATTR, and higher in early amyloidosis samples
Dorbala et al. [30]	^{18}F-florbetapir PET 60-min dynamic scan/ summed images at 10–60 min	4 ATTR 5 AL 5 Control	Visual assessment SUV Cardiac RI Myocardial TBR	•Uptake was noted in all cardiac amyloidosis patients and none in the control •TBR, RI, and myocardial-to-liver SUV can distinguish control from AL and ATTR
Osborne et al. [31]	^{18}F-florbetapir PET 30-min dynamic scan/ summed images over 0–3, 10–15, and 15–20 min	4 ATTR 4 AL 3 Controls	Visual assessment SUV	•Uptake was noted in all cardiac amyloidosis patients and none in the control •SUV able to differentiate CA vs control and AL vs ATTR
Manwani et al. [32]	^{18}F-florbetapir PET 60-min dynamic scan/ summed images at 0–60 min	15 AL	Visual assessment SUV Cardiac RI	•Uptake was noted in all cardiac amyloidosis •Suggesting that treatment-naïve patients may have higher cardiac uptake
Cuddy et al. [15]	^{18}F-florbetapir PET/CT 60-min dynamic scan/ summed images at 10–60 min	45 AL •25 AL-CA active •10 AL non-CA •10 AL-CA in remission	Visual assessment SUV Cardiac RI	•Active AL-CA had the highest amyloid burden based on RI •Evidence of cardiac amyloid was noted in AL non-CA patients; possible insight into preclinical disease process (using PET and ECV from CMR)

Table 4 Summarizing key studies of the diagnostic value of ^{18}F-florbetaben PET imaging for cardiac amyloidosis

	Acquisition	Patient cohort	Parameters	Notes
Law et al. [34]	^{18}F-florbetaben PET 80-min dynamic scan/summed images at 15–75 min	5 ATTRwt 5 AL 4 Control (hypertensive)	Visual assessment MTR Myocardium TBR	•Uptake was noted in all cardiac amyloidosis patients and none in the control •TBR and MTR higher in CA > control •MTR independent determinant of myocardial dysfunction in CA
Kircher et al. [35]	^{18}F-florbetaben PET 30-min dynamic scan/summed images at 10–30 min	5 ATTR 8 AL 1 AA 8 Control	Visual assessment MTR ΔMTR	•Retention pattern AL > AA > ATTR •MTR correlated with morphological and functional parameters (but not with cardiac biomarkers) •ΔMTR corresponded to treatment response during follow-up
Seo et al. [36]	^{18}F-florbetaben PET 20-min dynamic scan	6 AL 8 Control	Visual assessment SUV (max, mean, and ratio)	•Uptake was noted in all cardiac amyloidosis patients and none in the control •Can detect systemic amyloidosis and identify organ involvement
Genovesi et al. [37]	^{18}F-florbetaben PET 60-min dynamic scan/summed images at 5, 30, 50, and 110 min	20 ATTR (16 wt and 5v) 20 AL 20 Control	Visual assessment Cardiac RI Myocardium TBR SUV	•Uptake was noted in all cardiac amyloidosis patients and none in the control •Visual assessment and semiquantitative parameters were higher in AL > ATTR > controls

Table 5 Summarizing key studies of the diagnostic value of ^{18}F-NaF PET imaging for cardiac amyloidosis

	Acquisition	Patient cohort	Parameters	Notes
Van Der Gucht et al. [38]	^{18}F-NaF PET/CT 20 and 60 min	1 ATTRv (Val122Ile) 1 AL	Visual assessment Myocardium TBR	• M/B (early) 1.4 ATTR > 1.00 AL •No uptake noted in AL study
Gagliardi et al. [39]	^{18}F-NaF PET/CT 15 and 60 min	1 ATTRwt 1 ATTRv (Ile68Leu)	Visual assessment	• No uptake was noted in any scan phase in both patients
Trivieri et al. [41]	^{18}F-NaF PET/MR 15 and 90 min	4 ATTR (2 wt and 2 v) 3 AL 7 Control	Visual assessment Myocardium TBR	• $TBR_{max} > 0.84$ defined as the threshold to differentiate ATTR from AL
Morgenstern et al. [40]	^{18}F-NaF PET/CT 10 and 60 min	5 ATTR (3 wt and 2 v) 2 AL 5 Control	Visual assessment SUV_{mean}	• SUVm for ATTR patients was around 1.5*SUVm of controls and AL patients
Martineau et al. [43]	^{18}F-NaF PET/CT 60 and 90 min	7 ATTRwt 4 AL 3 Control	Visual assessment Myocardium TBR	• For diagnosis of ATTR, qualitative and quantitative assessments reported a sensitivity and specificity of 57%/100% vs 75%/100% respectively • *^{18}F-NaF PET/CT not ready for clinical use for cardiac amyloidosis*
Abulizi et al. [42]	^{18}F-NaF PET/MR 20 and 60 min	16 ATTR (7wt and 9v) 7 AL 4 Control	Visual assessment Myocardium TBR	• $TBR_{max} > 0.90$ is defined as the threshold to differentiate ATTR from AL • *Visual interpretation is challenging due to low contrast and faint uptake*

CA cardiac amyloidosis, *AL* light chain amyloidosis, *ATTR* cardiac transthyretin amyloidosis, *SUV* standardized uptake value, *RI* retention index, *LV* left ventricular, *TBR* target to background ratio, *ECV* extracellular volume: measured via cardiac magnetic resonance imaging)

Faint ^{18}F-NaF uptake reinforces the need for semiquantitative measures to differentiate ATTR from AL. Albeit low uptake values, target-to-background ratio (TBR_{mean}) recorded sensitivity and specificity of 75% and 100% respectively for a cutoff threshold of 0.89 for detection of ATTR (SUV_{mean} failed to show a significant difference between ATTR, AL, and controls consistent with the noted low visual uptakes) [43]. This is comparable to previously published semiquantitative M/B (TBR_{max}) ≥ 0.90 and 0.84 [41, 42].

As a bone-avid tracer, the hypothesized binding mechanism behind ^{18}F-NaF uptake in cardiac amyloidosis resembles more conventional bone-avid radiotracers compared to the previously discussed novel amyloid-binding tracers. ^{18}F-NaF can detect microcalcifications which form the basis of its use in cancer imaging. TTR amyloid fibrils are thought to bind more calcium compared to AL fibrils which might explain the differentiating capabilities of both ^{18}F-NaF and bone-avid radiotracers [11, 44].

Previous studies have shown that not all bone-seeking tracers are created equal with varied accuracy and clinical utility. Currently, available data on ^{18}F-NaF PET have shown inconsistent findings, weak visual uptake, and low TBG. A recent meta-analysis reported high specificity (100%) for ^{18}F-NaF PET but relatively low sensitivity (63%) [45]. However, the adequate judgment of its current clinical utility remains uncertain due to the limited available data regarding ^{18}F-NaF compared to its counterparts. Current literature (Table 1) has shown mixed methodology which could have contributed to the heterogeneity of the observed accuracy of ^{18}F-NaF. As such, larger comparative studies (against PYP or DPD) are needed to truly elucidate the role of ^{18}F-NaF PET in the workup of cardiac amyloidosis (Tables 2, 3, 4, and 5).

Coronary microvascular dysfunction (CMD)

The coronary microvasculature is comprised of coronary pre-arterioles and arterioles measuring < 500 µm in diameter and hold 90% of the total myocardial blood flow [46]. Although direct imaging of the coronary microvasculature is challenging, PET is at present the most accurate modality in clinical practice for the evaluation of coronary microvasculature function [47, 48].

Coronary microvascular dysfunction (CMD) is defined as ischemic cardiac chest pain with impairment in coronary microvascular blood flow in the absence of epicardial coronary obstruction. Although prevalence is unknown, several studies have shown how microvascular angina is not an uncommon initial presentation for patients with cardiac amyloidosis [49–51].

Autopsy studies have shown that amyloidosis causes microvascular dysfunction through three overlapping mechanisms: (1) deposition within vessel wall causing intimal thickening, (2) interstitial deposition causing perivascular compression, and (3) autonomic and/or endothelial dysfunction [52–55]. These contribute to ischemia and impaired

systolic dysfunction seen in some patients with cardiac amyloidosis.

Only one study has prospectively assessed microvascular dysfunction using PET MPI. Dorbala et al. prospectively enrolled 21 patients with cardiac amyloidosis (15 with light chain and 6 with transthyretin) and 10 patients with hypertensive left ventricular hypertrophy [56]. Amyloidosis was diagnosed with either endomyocardial biopsy ($n=10$) or extracardiac biopsy with echocardiography cardiac involvement ($n=11$). All patients underwent N-13 ammonia PET/CT imaging using standard imaging protocols. Microvascular dysfunction was defined as the presence of reduced peak stress myocardial blood flow (MBF), coronary flow reserve (CFR), or minima coronary vascular resistance.

Ischemic defect and transient ischemic dilatation were seen in 57% and 76% of the patients with amyloidosis. More importantly, stress MBF and MFR were significantly lower in those with amyloid compared to the LVH group (rest MBF 0.59 vs 0.88 ml/g/min $p=0.0004$; stress MBF 0.85 vs 1.85 ml/g/min $p<0.0001$; CFR 1.19 vs 2.23 $p<0.0001$ for amyloid vs LVH group respectively), and microvascular resistance was significantly higher (147 vs 117 ml/g/min/mm Hg $p=0.004$). Differences between the two groups were the same even after accounting for age, subclinical myocardial dysfunction, and lower left ventricular mass in the LVH group. Importantly, limitations of note were the small sample size, and how invasive angiography to rule out epicardial stenosis was done at a median of 164 from PET imaging.

Supplementary Information The online version contains supplementary material available at https://doi.org/10.1007/s10741-021-10183-w.

Data availability Not applicable.

Code availability Not applicable.

Declarations

Ethics approval and consent to participate Not applicable.

Consent for publication Not applicable.

Conflict of interests The authors declare no competing interests.

Additional declarations for articles in life science journals that report the results of studies involving humans and/or animals Not applicable.

References

1. Merlini G, Bellotti V (2003) Molecular mechanisms of amyloidosis. N Engl J Med 349(6):583–596
2. Phelan D et al (2012) Relative apical sparing of longitudinal strain using two-dimensional speckle-tracking echocardiography is both sensitive and specific for the diagnosis of cardiac amyloidosis. Heart 98(19):1442–1448
3. Syed IS et al (2010) Role of cardiac magnetic resonance imaging in the detection of cardiac amyloidosis. JACC Cardiovasc Imaging 3(2):155–164
4. Kristen AV, Dengler TJ, Katus HA (2007) Suspected cardiac amyloidosis: endomyocardial biopsy remains the diagnostic gold-standard. Am J Hematol 82(4):328
5. Falk RH, Quarta CC, Dorbala S (2014) How to image cardiac amyloidosis. Circ Cardiovasc Imaging 7(3):552–562
6. Lee SP et al (2020) Pittsburgh B compound positron emission tomography in patients with AL cardiac amyloidosis. J Am Coll Cardiol 75(4):380–390
7. Wechalekar AD, Gillmore JD, Hawkins PN (2016) Systemic amyloidosis. Lancet 387(10038):2641–2654
8. Alexander KM, Singh A, Falk RH (2017) Novel pharmacotherapies for cardiac amyloidosis. Pharmacol Ther 180:129–138
9. Perugini E et al (2005) Noninvasive etiologic diagnosis of cardiac amyloidosis using 99mTc-3,3-diphosphono-1,2-propanodicarboxylic acid scintigraphy. J Am Coll Cardiol 46(6):1076–1084
10. Ruberg FL et al (2019) Transthyretin amyloid cardiomyopathy: JACC state-of-the-art review. J Am Coll Cardiol 73(22):2872–2891
11. Castaño A, Bokhari S, Maurer MS (2015) Unveiling wild-type transthyretin cardiac amyloidosis as a significant and potentially modifiable cause of heart failure with preserved ejection fraction. Eur Heart J 36(38):2595–2597
12. Gillmore JD et al (2016) Nonbiopsy diagnosis of cardiac transthyretin amyloidosis. Circulation 133(24):2404–2412
13. Dorbala S et al (2019) ASNC/AHA/ASE/EANM/HFSA/ISA/SCMR/SNMMI expert consensus recommendations for multimodality imaging in cardiac amyloidosis: part 1 of 2—evidence base and standardized methods of imaging. J Nucl Cardiol 26(6):2065–2123
14. Rosengren S et al (2020) Diagnostic accuracy of [11C]PIB positron emission tomography for detection of cardiac amyloidosis. JACC Cardiovasc Imaging 13(6):1337–1347
15. Cuddy SAM et al (2020) Improved quantification of cardiac amyloid burden in systemic light chain amyloidosis: redefining early disease? JACC Cardiovasc Imaging 13(6):1325–1336
16. Castaño A et al (2016) Serial scanning with technetium pyrophosphate (99mTc-PYP) in advanced ATTR cardiac amyloidosis. Journal of Nuclear Cardiology: Official Publication of the American Society of Nuclear Cardiology 23(6):1355–1363
17. Klunk WE et al (2004) *Imaging brain amyloid in Alzheimer's disease with Pittsburgh compound-B*. Ann Neurol 55(3):306–319
18. Antoni G et al (2013) In vivo visualization of amyloid deposits in the heart with 11C-PIB and PET. J Nucl Med 54(2):213–220
19. Ezawa N et al (2018) Visualization of multiple organ amyloid involvement in systemic amyloidosis using (11)C-PiB PET imaging. Eur J Nucl Med Mol Imaging 45(3):452–461
20. Lee SP et al (2015) 11C-Pittsburgh B PET imaging in cardiac amyloidosis. JACC Cardiovasc Imaging 8(1):50–59
21. Kristen AV et al (2016) Cardiac amyloid load: a prognostic and predictive biomarker in patients with light-chain amyloidosis. J Am Coll Cardiol 68(1):13–24
22. Pilebro B et al (2018) Positron emission tomography (PET) utilizing Pittsburgh compound B (PIB) for detection of amyloid heart deposits in hereditary transthyretin amyloidosis (ATTR). J Nucl Cardiol 25(1):240–248
23. Koike H et al (2004) Pathology of early- vs late-onset TTR Met30 familial amyloid polyneuropathy. Neurology 63(1):129–138
24. Takasone K et al (2020) Non-invasive detection and differentiation of cardiac amyloidosis using (99m)Tc-pyrophosphate

scintigraphy and (11)C-Pittsburgh compound B PET imaging. Amyloid 27(4):266–274
25. Rosengren S et al (2020) Diagnostic accuracy of [(11)C]PIB positron emission tomography for detection of cardiac amyloidosis. JACC Cardiovasc Imaging 13(6):1337–1347
26. Choi SR et al (2012) Correlation of amyloid PET ligand florbetapir F 18 binding with Aβ aggregation and neuritic plaque deposition in postmortem brain tissue. Alzheimer Dis Assoc Disord 26(1):8–16
27. Ni R et al (2013) Amyloid tracers detect multiple binding sites in Alzheimer's disease brain tissue. Brain 136(7):2217–2227
28. Clark CM et al (2012) Cerebral PET with florbetapir compared with neuropathology at autopsy for detection of neuritic amyloid-β plaques: a prospective cohort study. Lancet Neurol 11(8):669–678
29. Park MA et al (2015) 18F-Florbetapir binds specifically to myocardial light chain and transthyretin amyloid deposits: autoradiography study. Circ Cardiovasc Imag 8(8)
30. Dorbala S et al (2014) Imaging cardiac amyloidosis: a pilot study using ^{18}F-florbetapir positron emission tomography. Eur J Nucl Med Mol Imaging 41(9):1652-1662
31. Osborne DR et al (2015) A routine PET/CT protocol with streamlined calculations for assessing cardiac amyloidosis using (18) F-florbetapir. Front Cardiovasc Med 2:23
32. Manwani R et al (2018) A pilot study demonstrating cardiac uptake with 18F-florbetapir PET in AL amyloidosis patients with cardiac involvement. Amyloid 25(4):247–252
33. Baratto L et al (2018) (18)F-Florbetaben whole-body PET/MRI for evaluation of systemic amyloid deposition. EJNMMI Res 8(1):66
34. Law WP et al (2016) Cardiac amyloid imaging with 18F-florbetaben PET: a pilot study. J Nucl Med 57(11):1733–1739
35. Kircher M et al (2019) Detection of cardiac amyloidosis with (18)F-florbetaben-PET/CT in comparison to echocardiography, cardiac MRI and DPD-scintigraphy. Eur J Nucl Med Mol Imaging 46(7):1407–1416
36. Seo M et al (2019) Clinical utility of 18F-florbetaben PET for detecting amyloidosis associated with multiple myeloma: a prospective case-control study. Clin Nucl Med 44(9):e503–e509
37. Genovesi D et al (2021) [18F]-Florbetaben PET/CT for differential diagnosis among cardiac immunoglobulin light chain, transthyretin amyloidosis, and mimicking conditions. JACC Cardiovasc Imaging 14(1):246–255
38. Van Der Gucht A et al (2016) [18F]-NaF PET/CT imaging in cardiac amyloidosis. Journal of Nuclear Cardiology: Official Publication of the American Society of Nuclear Cardiology 23(4):846–849
39. Gagliardi C et al (2017) Does the etiology of cardiac amyloidosis determine the myocardial uptake of [18F]-NaF PET/CT? Journal of Nuclear Cardiology: Official Publication of the American Society of Nuclear Cardiology 24(2):746–749
40. Morgenstern R et al (2018) 18Fluorine sodium fluoride positron emission tomography, a potential biomarker of transthyretin cardiac amyloidosis. Journal of Nuclear Cardiology: Official Publication of the American Society of Nuclear Cardiology 25(5):1559–1567
41. Trivieri MG et al (2016) (18)F-Sodium fluoride PET/MR for the assessment of cardiac amyloidosis. J Am Coll Cardiol 68(24):2712–2714
42. Abulizi M et al (2019) ^{18}F-Sodium fluoride PET/MRI myocardial imaging in patients with suspected cardiac amyloidosis. J Nuc Cardiol: Official Pub Am Soc Nuclear Cardiol
43. Martineau P et al (2021) Examining the sensitivity of 18F-NaF PET for the imaging of cardiac amyloidosis. Journal of Nuclear Cardiology: Official Publication of the American Society of Nuclear Cardiology 28(1):209–218
44. Masri A et al (2020) Molecular imaging of cardiac amyloidosis. Journal of Nuclear Medicine: Official Publication, Society of Nuclear Medicine 61(7):965–970
45. Kim SH, Kim YS, Kim S-J (2020) Diagnostic performance of PET for detection of cardiac amyloidosis: a systematic review and meta-analysis. J Cardiol 76(6):618–625
46. Gutterman DD et al (2016) The human microcirculation: regulation of flow and beyond. Circ Res 118(1):157–172
47. Bravo PE, Di Carli MF, Dorbala S (2017) Role of PET to evaluate coronary microvascular dysfunction in non-ischemic cardiomyopathies. Heart Fail Rev 22(4):455–464
48. Camici PG, d'Amati G, Rimoldi O (2015) Coronary microvascular dysfunction: mechanisms and functional assessment. Nat Rev Cardiol 12(1):48–62
49. Tsai SB et al (2011) Myocardial infarction with "clean coronaries" caused by amyloid light-chain AL amyloidosis: a case report and literature review. Amyloid: The Int J Exp Clinical Investigation: The Official J Int Soc Amyloidosis 18(3):160–164
50. Al Suwaidi J et al (1999) Systemic amyloidosis presenting with angina pectoris. Ann Intern Med 131(11):838–841
51. Ogawa H et al (2001) Cardiac amyloidosis presenting as microvascular angina–a case report. Angiology 52(4):273–278
52. Smith RR, Hutchins GM (1979) Ischemic heart disease secondary to amyloidosis of intramyocardial arteries. Am J Cardiol 44(3):413–417
53. Hongo M et al (2000) Comparison of electrocardiographic findings in patients with AL (primary) amyloidosis and in familial amyloid polyneuropathy and anginal pain and their relation to histopathologic findings. Am J Cardiol 85(7):849–853
54. Modesto KM et al (2007) Vascular abnormalities in primary amyloidosis. Eur Heart J 28(8):1019–1024
55. Buja LM, Khoi NB, Roberts WC (1970) Clinically significant cardiac amyloidosis. Clinicopathologic findings in 15 patients. The Am J Cardiol 26(4):94–405
56. Dorbala S et al (2014) Coronary microvascular dysfunction is related to abnormalities in myocardial structure and function in cardiac amyloidosis. JACC Heart failure 2(4):358–367
57. Takasone K et al (2020) Non-invasive detection and differentiation of cardiac amyloidosis using 99mTc-pyrophosphate scintigraphy and 11C-Pittsburgh compound B PET imaging. Amyloid 27(4):266–274